AGH

AGH University of Science and Technology

FIELD OF SCIENCE: NATURAL SCIENCES

SCIENTIFIC DISCIPLINE: PHYSICAL SCIENCES

DOCTORAL THESIS

Exploration of Baryon Number Factorial Cumulants in the Context of the Quantum Chromodynamics Phase Diagram

Author: Michał Barej

Supervisor: Prof. Adam Bzdak

Completed in: Faculty of Physics and Applied Computer Science

Kraków, 2023

Declaration of the Author of this dissertation:

Aware of legal responsibility for making untrue statements I hereby declare that I have written this dissertation myself and all the contents of the dissertation have been obtained by legal means.

.....

Date, Author's signature

Declaration of the thesis Supervisor:

This dissertation is ready to be reviewed.

.....

Date, Supervisor's signature

Acknowledgments

I want to thank my Supervisor, Prof. Adam Bzdak. This doctoral thesis would never have been completed without his creative ideas and guidance. I am grateful to him for the numerous discussions and readiness to help. He taught me how to read and write scientific papers. Prof. Bzdak is a supervisor I wish to everybody.

I also appreciated scientific and private conversations with other doctoral students at AGH University as well as during conferences and scientific schools.

I want to thank my Parents who have always supported me and believed in my abilities. Special thanks go to my wife, Agnieszka, who was on the frontline listening about my everyday struggles and little successes in science.

The research described in this doctoral thesis was partially supported by the Ministry of Science and Higher Education (PL) and by the National Science Centre (PL), Grant No. 2018/30/Q/ST2/00101.

Abstract

The strongly interacting matter phase diagram is not yet well explored. In particular, the search for the expected phase transition and critical point between the hadronic gas (protons, neutrons, etc.) and the quark-gluon plasma (deconfined quarks and gluons) is one of the greatest challenges in nuclear and high-energy physics nowadays. Theoretical studies predict that the fluctuations in the baryon number, electric charge, and strangeness are sensitive to such a transition and critical point. These fluctuations are quantified by the cumulants, factorial cumulants, and factorial moments which are measured experimentally at the major particle collider facilities. The cumulants naturally appear in statistical mechanics and lattice numerical calculations. On the other hand, factorial cumulants are useful when investigating multiparticle correlations. The recent results of the STAR and HADES collaborations might be interpreted as a signature of the critical phenomena. However, greater statistics as well as a careful study of various effects such as baryon number conservation or volume fluctuations are needed.

In this thesis, the cumulants and factorial cumulants originating from various effects are calculated analytically. First of all, the mixed proton-antiproton factorial cumulants from global baryon number conservation are obtained. They include more information than often studied net-proton cumulants. What is more, they might be helpful in distinguishing between the effects of the baryon annihilation with local baryon number conservation law and another scenario assuming global baryon number conservation only. Then, in this dissertation, the baryon number cumulants and factorial cumulants in the subsystem are obtained assuming the global baryon number conservation and short-range correlations. The fact that they are expressed by the cumulants without baryon number conservation can enable correcting the experimental data or numerical results for this effect. In the next step, a method of calculating corrections to the cumulants from baryon number conservation and short-range correlations is developed. It is especially important for small systems. In the last part, the cumulants and factorial cumulants due to fluctuations in the width of the proton rapidity density distribution are derived. They are expected to be caused, e.g., by the event-by-event fluctuations in the energy deposition of stopped protons resulting in longitudinal fluctuations of the fireball density. This effect is found to be potentially important when studying proton or baryon number cumulants.

Streszczenie

Diagram fazowy materii oddziałującej silnie nie jest jeszcze dobrze zbadany. W szczególności poszukiwanie spodziewanego przejścia fazowego i punktu krytycznego pomiędzy gazem hadronowym (protony, neutrony itp.) i plazmą kwarkowo-gluonową (nieuwięzione kwarki i gluony) jest jednym z największych wyzwań w dzisiejszej fizyce jądrowej i fizyce wysokich energii. Badania teoretyczne przewidują, że fluktuacje liczby barionowej, ładunku elektrycznego i dziwności są czułe na takie przejście fazowe i punkt krytyczny. Te fluktuacje są opisywane ilościowo przez kumulanty faktorialne, kumulanty i momenty faktorialne, które są mierzone eksperymentalnie w największych zderzaczach cząstek. Kumulanty naturalnie pojawiają się w mechanice statystycznej oraz obliczeniach numerycznych na sieciach. Z drugiej strony kumulanty faktorialne są użyteczne w badaniu korelacji wielocząstkowych. Najnowsze wyniki kolaboracji STAR i HADES mogą być interpretowane jako przejaw zjawisk krytycznych. Jednakże potrzebna jest zarówno większa statystyka, jak i staranne zbadanie różnych efektów, takich jak zasada zachowania liczby barionowej, czy fluktuacje objętości.

W niniejszej rozprawie obliczono analitycznie kumulanty faktorialne i kumulanty pochodzące z różnych efektów. Najpierw otrzymano mieszane protonowo-antyprotonowe kumulanty faktorialne z globalnej zasady zachowania liczby barionowej. Zawierają one więcej informacji niż często badane kumulanty wypadkowej liczby protonowej. Co więcej, mogą one być pomocne w rozróżnieniu pomiędzy efektami anihilacji barionów z lokalnym zachowaniem liczby barionowej i innym scenariuszem zakładającym tylko globalne zachowanie liczby barionowej. Następnie w tej rozprawie otrzymano kumulanty faktorialne i kumulanty liczby barionowej w części układu, zakładając globalne zachowanie liczby barionowej oraz korelacje krótkozasięgowe. Fakt, że kumulanty te są wyrażone przez kumulanty bez zachowania liczby barionowej, może pozwolić na uwzględnienie tego efektu przy korygowaniu danych eksperymentalnych lub wyników numerycznych. W kolejnym kroku opracowano metodę obliczania poprawek do kumulantów z zachowania liczby barionowej i korelacji krótkozasięgowych. Jest to ważne szczególnie dla małych układów. W ostatniej części wyprowadzono wzory na kumulanty faktorialne i kumulanty wynikające z fluktuacji szerokości rozkładu gęstości protonów w pośpieszności (ang. *rapidity*). Spodziewać się można, że są one spowodowane na przykład fluktuacjami energii deponowanej przez zatrzymane protony. Skutkują one podłużnymi fluktuacjami gęstości gorącej materii. Zauważono, że ten efekt jest potencjalnie ważny w badaniu kumulantów liczby protonowej lub barionowej.

Contents

Chapter 1

Thesis structure

The central part of this doctoral thesis consists of a collection of four published articles. They present analytical calculations of the proton and baryon number cumulants and factorial cumulants originating from different effects. These effects should be taken into account when analyzing experimental data from relativistic heavy-ion collisions in the context of the search for the predicted phase transition and critical point between hadronic matter and quark-gluon plasma. The articles are listed below.

Article 1: **M. Barej** and A. Bzdak, *Factorial cumulants from global baryon number conservation*, Phys. Rev. C 102, no. 6, 064908 (2020). DOI:10.1103/PhysRevC.102.064908.

Article 2: **M. Barej** and A. Bzdak, *Factorial cumulants from short-range correlations and global baryon number conservation*, Phys. Rev. C 106, no. 2, 024904 (2022). DOI:10.1103/PhysRevC.106.024904.

Article 3: **M. Barej** and A. Bzdak, *Cumulants from short-range correlations and baryon number conservation at next-to-leading order*, Phys. Rev. C 107, no. 3, 034914 (2023). DOI:10.1103/PhysRevC.107.034914.

Article 4: **M. Barej** and A. Bzdak, *Cumulants from fluctuating width of rapidity distribution*, Phys. Rev. C 108, no. 1, 014907 (2023). DOI:10.1103/PhysRevC.108.014907.

The thesis begins with the introduction where the quantum chromodynamics (QCD) phase diagram is discussed. Then, the measures of fluctuations and correlations, i.e., cumulants, factorial cumulants, and factorial moments are explained in the context of particle multiplicity distribution in heavy-ion collisions. This is followed by an overview of the selected recent theoretical and experimental results. Finally, the goal of this thesis is presented. The next chapter constitutes a guide to the articles. For each article, its content is summarized with a focus on its aim, assumptions, and main findings. The last chapter is a summary of the thesis. In the appendixes, the supplemental information is included and the articles are attached.

Chapter 2

Introduction

2.1 The QCD phase diagram

The understanding of matter and its different phases is one of the most fundamental problems in science. Different phases of matter and conditions governing the transitions between them can be summarized in the phase diagrams. The temperature–pressure phase diagram of water is perhaps the best-known one. It shows the ranges of temperature and pressure when the water is solid (ice), liquid, or gaseous (water vapor). The research discussed in this thesis is related to the phase diagram of the strongly interacting matter, known as the quantum chromodynamics (QCD) phase diagram, which is not yet well explored [1].

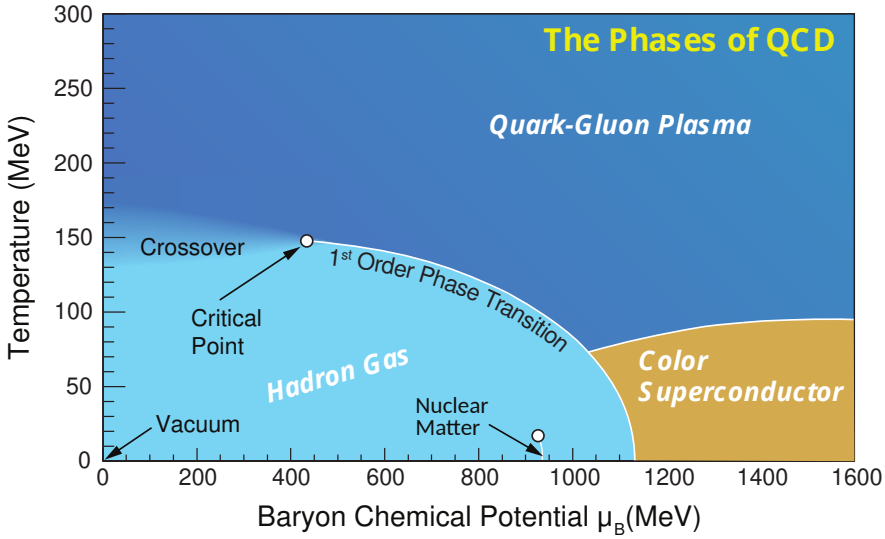

Figure 2.1: The conjectured QCD phase diagram with the predicted first-order phase transition and corresponding critical endpoint [1, 2].

The conjectured QCD phase diagram is shown in Fig. 2.1. It is the temperature–baryon chemical potential ($T - \mu_B$) diagram. The baryon chemical potential is the chemical potential for baryons.[1] It is commonly

[1]The chemical potential can be defined as $\mu = \partial E/\partial .N|_{S,V}$, where E is the system energy, N is the number of particles, S is the entropy, and V is the volume. Therefore, its meaning is the energy cost to add an *infinitesimal* number of particles to the system while its entropy and volume are fixed [3].

known that the regular nuclear matter building up the atomic nuclei consists of protons and neutrons. The protons and neutrons, being hadrons, consist of quarks and gluons. Under typical conditions, quarks and gluons are always confined in hadrons. However, they can be deconfined at very high temperatures. It is believed that the early Universe was filled with deconfined quarks and gluons, the quark-gluon plasma (QGP) state. There are signatures of strongly interacting QGP created for an enormously short time in a tiny volume in the relativistic heavy-ion collisions at the Relativistic Heavy Ion Collider (RHIC) of Brookhaven National Laboratory (BNL), at the Super Proton Synchrotron (SPS), and the Large Hadron Collider (LHC) of the European Organization for Nuclear Research (CERN). These signatures include the azimuthal asymmetry of particle production, known as elliptic flow, triangular flow, and others [4, 5], the jet quenching effect [6, 7], and the strangeness enhancement [8–10].

It is conjectured that at low temperatures and extremely high μ_B, corresponding to high densities, a matter consisting mostly of neutrons is deconfined into quarks. Under these conditions, the quark pairs (analogous to Cooper pairs in superconductivity) are expected to be formed due to attractive strong interaction between two quarks. Perhaps, such a phase of color superconductivity is created in the core of a neutron star [11–13].

The Lattice QCD numerical calculations showed that at $\mu_B \approx 0$, there is a rapid but continuous crossover between the hadronic matter and QGP with a pseudo-critical temperature of about 155 MeV [14, 15]. This is seen from the fast increase of the energy density and entropy density when increasing temperature.

Most of the regions of the QCD phase diagram are not accessible by pure QCD theory because it becomes non-perturbative there. Due to the so-called sign problem [16], Lattice QCD methods are limited to a small μ_B regime. Most of the experiments at the LHC and RHIC also reproduce the conditions of nearly vanishing baryon chemical potential. Consequently, the QCD phase diagram regions with greater μ_B are still not well known [1]. Nevertheless, many effective models predict a first-order phase transition with the corresponding critical endpoint between the hadronic matter and the quark-gluon plasma [13, 17–20]. Nowadays, there is a big effort, both theoretical and experimental, to search for this phase transition.

Baryons are always produced as baryon-antibaryon pairs satisfying the baryon number conservation law. In the heavy-ion collision experiments at high energies (LHC energies and top RHIC energies), there are many baryon-antibaryon pairs produced. Consequently, the number of baryons is approximately the same as the number of antibaryons. This situation corresponds to the vanishing baryon chemical potential. At lower collision energies, fewer pairs are created. The incoming baryons (from the incoming nuclei) that are stopped in the acceptance region contribute more to the total baryon number. Therefore, there are more baryons than antibaryons in the system. This results in greater μ_B. Consequently, heavy-ion collisions at different energies allow the exploration of different regions of the QCD phase diagram. Such experiments include, e.g., the Beam Energy Scan program at RHIC [21–23] and the heavy-ion program of the NA61/SHINE Collaboration at the CERN SPS [24–26]. There are also hopes for interesting results from future experiments at the Facility for Antiproton and Ion Research (FAIR) of the GSI Helmholtz Center for Heavy Ion Research [27].

At this point, it should be mentioned that understanding heavy-ion collision experiments is challenging. The two atomic nuclei are accelerated to almost the speed of light, thus they are Lorentz-contracted. They collide and, in the overlapping zone, the quark-gluon plasma is likely created, thanks to the enormous

energy density. Then, the QGP expands and cools down. At some point (about 155 MeV for $\mu_B = 0$), the hadronization happens - the quarks and gluons become again confined into hadrons such as pions, kaons, protons, antiprotons, etc. The system further expands. Subsequently, the chemical freeze-out takes place. This means that the abundances of particles are frozen - there is no longer inelastic scattering between the hadrons. Then, in the kinetic freeze-out, the momenta of the particles become frozen - there is no more elastic scattering. All these phenomena happen within approximately 10 fm/c (which corresponds to about 3×10^{-23} s). Because of the extreme conditions, none of these processes can be accessed directly. All the experimental information is obtained from the particles observed at the complicated detector systems where they reach approximately 10^{15} fm/c (about 3×10^{-9} s) after the collision. The detectors in modern experiments consist of many parts aiming to detect different kinds of particles. They are equipped with advanced electronic and triggering systems. The physical conclusions from the experiments can be obtained only after sophisticated analysis of the huge amounts of collected data.

One of the simplest models to study the phase transitions and critical points is the Ising model applied to magnetism. In this model, the system consists of the lattice of many spins; each of them can be pointing either up or down. The energy of each spin depends on its state, the states of its nearest neighbors, and the external magnetic field, h. The total energy is minimized when all the spins are aligned in the same direction. The Ising model is usually studied with the mean field approximation. At $T = 0$, the system is in its ground state. Namely, either all of the spins are up or all are down, depending on h. Therefore, there is a sudden jump in the average magnetization (magnetization can be thought of as a balance between spins up and down) when crossing $h = 0$. When the temperature grows, some of the spins in the system change their orientation due to thermal fluctuations. Thus, the difference in magnetization when crossing $h = 0$ is still sharp but smaller. Eventually, at the critical temperature, T_c, recognized in this context as the Curie temperature[2], this difference decreases to zero and there is a smooth transition between $h > 0$ and $h < 0$, see Fig. 2.2. This means that the difference between the properties of the two states disappears. At $h = 0$ and $T < T_c$, there is the first-order phase transition between negative and positive average magnetization. At $h = 0$ and $T > T_c$, there is a crossover. $(h = 0, T = T_c)$ is the critical point. The mathematical similarity in the description of the phase transition and critical phenomena in different systems is well-known in physics. Therefore, a similar behavior is expected also in the case of the QCD phase diagram. As mentioned earlier, the smooth crossover is known to appear in the QCD phase diagram at a small μ_B. Thus, the predicted first-order phase transition has to end somewhere with the critical point where it transforms into the crossover.

In general, the phase transition is the coexistence of two phases, e.g., the coexistence of water and ice or of water and water vapor. Consider water in an open container. Let us focus on a little subsystem of the water volume. At $0°C < T < 100°C$, the probability distribution $P(N)$ of having N water molecules in the subvolume is expected to be a unimodal distribution. At higher temperatures, there can be only water vapor in the subvolume. Consequently, $P(N)$ would be also a unimodal distribution with a peak at lower N due to the lower density of molecules in vapor than in water. At $T = 100°C$, the water is boiling and the vapor bubbles are appearing in the volume of water. The two states coexist. Therefore, one can expect a bimodal $P(N)$ distribution. Following this reasoning, the model of two-component distribution,

[2]Typically, a material is a ferromagnet at $T < T_c$ and a paramagnet at $T > T_c$.

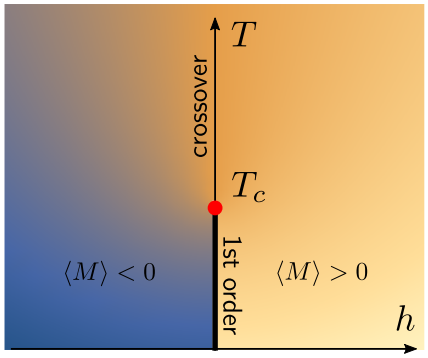

Figure 2.2: The phase diagram of the magnetic system in the Ising model [1].

$P(N) = (1-\alpha)P_A(N) + \alpha P_B(N)$, where $0 < \alpha < 1$, was proposed in Ref. [28] where it was also shown that even a very small α can result in large higher-order cumulants. Recently, this model was tested by the STAR Collaboration [23]. No two-component structure is observed at collision energies per nucleon-nucleon pair, $\sqrt{s_{NN}} \geq 11.5\,\text{GeV}$. No conclusions can be drawn for lower energies yet. This potentially is a method to put a limit on the location of the predicted critical point, suggesting that it may be observed at $\sqrt{s_{NN}} < 11.5$ GeV corresponding to greater μ_B. However, the modifications of the probability distribution are likely very tiny. Hence, sensitive measures of the fluctuations of its shape should be used. These measures are discussed in the next section.

2.2 Correlations and fluctuations

The results of statistical mechanics obtained, e.g., within the Ising model apply also to other phase transitions. For instance, some quantities change in a common way when approaching the critical point, e.g., they are proportional to $(T - T_c)^\gamma$, where T_c is a critical temperature and γ is a critical exponent. It is also known that the correlation length grows near the critical point. This results in an increase in the fluctuations of the quantities relevant to the discussed medium. In the case of the strongly interacting matter, when approaching the critical point, an increase in fluctuations of the net-baryon number, electric charge, and strangeness is expected [1, 29–41]. These fluctuations are most often described by the cumulants, κ_m, factorial cumulants, $\hat{C}_m$, and factorial moments, F_m [1, 42].

The probability generating function for the discrete probability distribution $P(n)$ is given by

$$H(z) = \sum_{n=0}^{\infty} P(n) z^n \,. \tag{2.1}$$

$P(n)$ in this context is the probability of producing or observing n particles of one kind in a heavy-ion collision. The mth factorial moment is defined as

$$F_m = \left\langle \frac{n!}{(n-m)!} \right\rangle \,, \tag{2.2}$$

where $\langle x \rangle = \sum_{n=0}^{\infty} x P(n)$ is the expected value of x. F_m can be calculated from $H(z)$:

$$F_m = \left. \frac{d^m H(z)}{dz^m} \right|_{z=1} \,. \tag{2.3}$$

Moreover, F_m is the integrated m-particle rapidity[3] density distribution, ϱ_m, [43]

$$F_m = \int dy_1 dy_2 \dots dy_m \, \varrho_m(y_1, y_2, \dots, y_m) \,. \tag{2.4}$$

The cumulants are obtained from the cumulant generating function, $K(t)$:

$$K(t) = \ln \left[\sum_{n=0}^{\infty} P(n) e^{tn} \right] = \sum_{m=1}^{\infty} \frac{t^m}{m!} \kappa_m \,. \tag{2.5}$$

Therefore, the mth cumulant can be calculated using the mth derivative of $K(t)$:

$$\kappa_m = \left. \frac{d^m K(t)}{dt^m} \right|_{t=0} \,. \tag{2.6}$$

The mth central moment is defined in probability theory as

$$\mu_m = \langle (n - \langle n \rangle)^m \rangle \,. \tag{2.7}$$

The central moments can be obtained from the relevant central moment generating function,

$$C(t) = \sum_{n=0}^{\infty} P(n) e^{t(n - \langle n \rangle)} \quad \Rightarrow \quad \mu_m = \left. \frac{d^m C(t)}{dt^m} \right|_{t=0} \,. \tag{2.8}$$

The cumulants are related to central moments. Namely, from Eqs. (2.5) and (2.8),

$$K(t) = \ln[C(t)] + t\langle n \rangle \,. \tag{2.9}$$

From this one obtains

$$\begin{aligned} \kappa_1 &= \langle n \rangle \,, \\ \kappa_m &= \sum_{k=1}^{m} (-1)^{k-1} (k-1)! \, \text{Bell}_{m,k}(0, \mu_2, \mu_3, ..., \mu_{m-k+1}) \,, \quad m > 1 \,, \end{aligned} \tag{2.10}$$

where the result for $m > 1$ is obtained using Faà di Bruno's formula and $\text{Bell}_{m,k}$ are the partial exponential Bell polynomials. In particular, the first four cumulants read

$$\begin{aligned} \kappa_1 &= \langle n \rangle \,, \\ \kappa_2 &= \mu_2 \,, \\ \kappa_3 &= \mu_3 \,, \\ \kappa_4 &= \mu_4 - 3\mu_2^2 \,. \end{aligned} \tag{2.11}$$

Therefore, the quantities describing the shape of the probability distribution can be expressed by cumulants, i.e., the expected value: $\langle n \rangle = \kappa_1$, the variance: $\sigma^2 = \mu_2 = \kappa_2$, the skewness: $S = \mu_3/\sigma^3 = \kappa_3/\kappa_2^{3/2}$, and

[3] Here the formalism is presented in terms of rapidity densities and rapidity correlation functions because rapidity is the variable commonly used in the analysis of the heavy-ion collisions experimental data. However, other variables can be used instead of rapidity. For completeness, the rapidity is defined as $y = \frac{1}{2} \ln \left(\frac{E + p_z}{E - p_z} \right)$, where E is the particle energy, p_z is its longitudinal momentum (momentum along the axis determined by the incoming nuclei motion), and the speed of light $c = 1$.

the kurtosis[4]: $\kappa = \mu_4/\sigma^4 - 3 = \kappa_4/\kappa_2^2$. From this, the interpretation of the following cumulant ratios is seen,

$$\begin{aligned} \frac{\kappa_2}{\kappa_1} &= \frac{\sigma^2}{\langle n \rangle} \quad \text{(scaled variance)}\,, \\ \frac{\kappa_3}{\kappa_2} &= S\sigma \quad \text{(scaled skewness)}\,, \\ \frac{\kappa_4}{\kappa_2} &= \kappa\sigma^2 \quad \text{(scaled kurtosis)}\,. \end{aligned} \tag{2.12}$$

The particle number cumulants also appear in statistical mechanics, in the grand-canonical ensemble. Here, the mth scaled susceptibility is defined as [44, 45]

$$\chi_m = \frac{\partial^m \left(P/T^4\right)}{\partial \left(\mu_B/T\right)^m} = \frac{\kappa_m}{VT^3}\,, \tag{2.13}$$

where P is pressure, T is temperature, V is volume, and μ_B is baryon chemical potential. Therefore, the cumulant ratio is equivalent to the scaled susceptibility ratio,

$$\frac{\chi_m}{\chi_l} = \frac{\kappa_m}{\kappa_l} \tag{2.14}$$

for any positive integers m and l. The cumulants naturally appear not only in statistical mechanics but also in Lattice QCD calculations [14, 36, 46]. For these reasons, the cumulant ratios are often measured experimentally, see, e.g., Refs. [47–52].

The factorial cumulant generating function, $G(z)$, reads

$$G(z) = \ln\left[\sum_{n=0}^{\infty} P(n) z^n\right] = \sum_{m=1}^{\infty} \frac{(z-1)^m}{m!} \hat{C}_m\,. \tag{2.15}$$

By analogy to cumulants, the mth factorial cumulant, $\hat{C}_m$, is calculated using $G(z)$:

$$\hat{C}_m = \left.\frac{d^m G(z)}{dz^m}\right|_{z=1}\,. \tag{2.16}$$

The factorial cumulants represent the integrated multiparticle correlation functions [1, 53–55]. This fact can be seen as follows. The second factorial cumulant obtained by straightforward calculation from Eq. (2.16) reads

$$\hat{C}_2 = \langle n(n-1) \rangle - \langle n \rangle^2\,. \tag{2.17}$$

On the other hand, the two-particle rapidity density distribution, $\varrho_2(y_1, y_2)$, is given by

$$\varrho_2(y_1, y_2) = \varrho(y_1)\varrho(y_2) + C_2(y_1, y_2)\,, \tag{2.18}$$

where $\varrho(y)$ is the single-particle rapidity density and $C_2(y_1, y_2)$ is the two-particle rapidity correlation function. Integrating both sides of this equation, one obtains

$$\int dy_1 dy_2\, \varrho_2(y_1, y_2) = \int dy_1\, \varrho(y_1) \int dy_2\, \varrho(y_2) + \int dy_1 dy_2\, C_2(y_1, y_2)\,, \tag{2.19}$$

[4]The kurtosis is often defined as μ_4/σ^4. This gives three for the normal distribution. Therefore, it is convenient to define kurtosis as presented in the main text so that $\kappa = 0$ for the normal distribution.

which is, by Eqs. (2.4) and (2.2),

$$\langle n(n-1)\rangle = \langle n\rangle^2 + \int dy_1 dy_2\, C_2(y_1, y_2)\,. \tag{2.20}$$

Therefore, by comparison of Eqs. (2.17) and (2.20), the second factorial cumulant is indeed the integrated two-particle correlation function,

$$\hat{C}_2 = \int dy_1 dy_2\, C_2(y_1, y_2)\,. \tag{2.21}$$

The analogous relations are also found for higher-order factorial cumulants. Namely,

$$\hat{C}_m = \int dy_1 dy_2 \ldots dy_m\, C_m(y_1, y_2, \ldots, y_m)\,, \tag{2.22}$$

where $C_m(y_1, y_2, \ldots, y_m)$ is the m-particle *genuine* correlation function, which means that the contributions of the lower-order correlations are subtracted, e.g., for the three-particle correlation function:

$$\begin{aligned} C_3(y_1, y_2, y_3) = \varrho_3(y_1, y_2, y_3) - \varrho(y_1)\varrho(y_2)\varrho(y_3) \\ - \varrho(y_1)C_2(y_2, y_3) - \varrho(y_2)C_2(y_1, y_3) - \varrho(y_3)C_2(y_1, y_2)\,. \end{aligned} \tag{2.23}$$

The formulas for the higher-order genuine correlation functions can be found, e.g., in Ref. [56].

The cumulants, κ_m, mix correlation functions of different orders as seen from the relation in which the mth cumulant can be obtained from the factorial cumulants of different orders,

$$\kappa_m = \sum_{k=1}^{m} S(m,k)\hat{C}_k\,, \tag{2.24}$$

where $S(m,k)$ are the Stirling numbers of the second kind. Hence, the factorial cumulants are easier to interpret in terms of multiparticle correlations. Eq. (2.24) has been discussed in Ref. [57]. For the first four cumulants, it reads:

$$\begin{aligned} \kappa_1 &= \langle n\rangle = \hat{C}_1\,, \\ \kappa_2 &= \langle n\rangle + \hat{C}_2\,, \\ \kappa_3 &= \langle n\rangle + 3\hat{C}_2 + \hat{C}_3\,, \\ \kappa_4 &= \langle n\rangle + 7\hat{C}_2 + 6\hat{C}_3 + \hat{C}_4\,. \end{aligned} \tag{2.25}$$

Obviously, one can invert this relation and calculate the mth factorial cumulant from the cumulants [57]. The application of factorial cumulants has also provided important experimental results [22, 23, 58, 59].

The Poisson distribution,

$$P(n) = \frac{e^{-\langle n\rangle}\langle n\rangle^n}{n!}\,, \tag{2.26}$$

is an important special case. A straightforward calculation using Eq. (2.15) gives the factorial cumulant generating function

$$G(z) = \langle n\rangle(z-1)\,. \tag{2.27}$$

Hence, the factorial cumulants are given by, see Eq. (2.16),

$$\begin{aligned} \hat{C}_1 &= \langle n\rangle\,, \\ \hat{C}_m &= 0\,, \quad m > 1\,. \end{aligned} \tag{2.28}$$

This indicates that if the number of particles follows the Poisson distribution, there are no multiparticle correlations in the system. In the language of factorial moments, applying Eqs. (2.1) and (2.3), one obtains $F_m = \langle n \rangle^m$, whereas all the cumulants of the Poisson distribution are equal to the expected value,

$$\kappa_m = \langle n \rangle \,. \tag{2.29}$$

Hence, every cumulant ratio

$$\frac{\kappa_m}{\kappa_l} = 1 \,. \tag{2.30}$$

The Poisson distribution constitutes the baseline of the no-correlations case.

For the net-proton number, $n = (n_p - n_{\bar{p}})$ (with n_p and $n_{\bar{p}}$ being the number of protons and antiprotons, respectively), the relevant baseline is obtained from the Skellam distribution, which is the distribution of the difference between two Poissonian random variables. Namely,

$$P(n) = \sum_{n_p=0}^{\infty} \sum_{n_{\bar{p}}=0}^{\infty} P_1(n_p) P_2(n_{\bar{p}}) \delta_{n_p - n_{\bar{p}}, n} \,, \tag{2.31}$$

where P_1 and P_2 are the Poisson distributions with means $\langle n_p \rangle$ and $\langle n_{\bar{p}} \rangle$, respectively. The Kronecker delta requires the constraint that n is a difference between two variables. Eq. (2.31) leads to

$$P(n) = e^{-(\langle n_p \rangle + \langle n_{\bar{p}} \rangle)} \left(\frac{\langle n_p \rangle}{\langle n_{\bar{p}} \rangle} \right)^{n/2} I_n \left(2\sqrt{\langle n_p \rangle \langle n_{\bar{p}} \rangle} \right) \,, \tag{2.32}$$

where

$$I_n(x) = \sum_{m=0}^{\infty} \frac{1}{m!(m+n)!} \left(\frac{x}{2} \right)^{2m+n} \tag{2.33}$$

is a modified Bessel function of the first kind.

The multiparticle correlations are called short-range correlations if the correlations are local in, say, rapidity. Usually, short-range rapidity correlations depend solely on relative distances between particles and they are significant only when this distance is small [54]. In this case, each factorial cumulant, $\hat{C}_m$, is proportional to the mean number of particles, $\langle n \rangle$, and to the range in rapidity, Δy. Therefore, the mth cumulant, κ_m, is also proportional to $\langle n \rangle$, so the cumulant ratios, κ_m / κ_l, are constant with respect to $\langle n \rangle$. By contrast, the long-range correlations are the correlations that are constant over the whole rapidity region. It turns out that for long-range correlations, $\hat{C}_m$ scales as $\langle n \rangle^m$ and as $(\Delta y)^m$. Therefore, κ_m is a linear combination of $\langle n \rangle^k$, $k = 1, 2, ..., m$, and the cumulant ratios, κ_m / κ_l, are the ratios of such polynomials.

The factorial moments, cumulants, and factorial cumulants can be generalized to the case of multiple variables. In particular, the factorial cumulant generating function for the bivariate discrete probability distribution, $P(n_p, n_{\bar{p}})$, is defined as

$$G(z, \bar{z}) = \ln \left[\sum_{n_p=0}^{\infty} \sum_{n_{\bar{p}}=0}^{\infty} P(n_p, n_{\bar{p}}) z^{n_p} \bar{z}^{n_{\bar{p}}} \right] \,. \tag{2.34}$$

In terms of heavy-ion physics, n_p and $n_{\bar{p}}$ can be interpreted as the numbers of two species of particles, e.g., protons and antiprotons. From this, one can calculate the (m, l) factorial cumulant corresponding to the correlation of m particles of the first kind (protons) and l particles of the second kind (antiprotons),

$$\hat{C}^{(m,l)} = \frac{\partial^m}{\partial z^m} \frac{\partial^l}{\partial \bar{z}^l} G(z, \bar{z}) \bigg|_{z=\bar{z}=1} \,. \tag{2.35}$$

For instance, $\hat{C}^{(1,1)}$ is the integrated one proton – one antiproton correlation function.

By analogy, the cumulant generating function of two variables (for two kinds of particles) is given by

$$K(t,\bar{t}) = \ln\left[\sum_{n_p=0}^{\infty}\sum_{n_{\bar{p}}=0}^{\infty} P(n_p,n_{\bar{p}})e^{tn_p}e^{\bar{t}n_{\bar{p}}}\right] . \tag{2.36}$$

Net-proton cumulants are often measured experimentally, see, e.g., Refs. [52, 59]. When substituting $\bar{t} = -t$ into Eq. (2.36), one obtains

$$K(t,-t) = \ln\left[\sum_{n_p=0}^{\infty}\sum_{n_{\bar{p}}=0}^{\infty} P(n_p,n_{\bar{p}})e^{t(n_p-n_{\bar{p}})}\right] \tag{2.37}$$

and

$$\kappa_m(n_p - n_{\bar{p}}) = \left.\frac{d^m K(t,-t)}{dt^m}\right|_{t=0} \tag{2.38}$$

is the mth net-proton cumulant. For example,

$$\begin{aligned}
\kappa_1(\Delta n) &= \langle \Delta n \rangle \,, \\
\kappa_2(\Delta n) &= \langle (\Delta n - \langle \Delta n \rangle)^2 \rangle \,, \\
\kappa_3(\Delta n) &= \langle (\Delta n - \langle \Delta n \rangle)^3 \rangle \,, \\
\kappa_4(\Delta n) &= \langle (\Delta n - \langle \Delta n \rangle)^4 \rangle - 3\langle (\Delta n - \langle \Delta n \rangle)^2 \rangle^2 \,,
\end{aligned} \tag{2.39}$$

where $\Delta n = n_p - n_{\bar{p}}$ and $\langle ... \rangle$ means averaging over $P(n_p, n_{\bar{p}})$. Note that these relations are analogous to those given in Eqs. (2.11).

2.3 Selected recent results

For the measurements of the proton (or baryon) number cumulants and factorial cumulants, the first step in the search for the expected first-order phase transition and critical point is to observe any deviations from the Poisson (Skellam for net-protons or net-baryons) baseline. It is predicted that near the critical point, the deviations of the cumulants from the noncritical baseline will depend non-monotonically on the collision energy [30, 35, 38, 60, 61].

The NA61/SHINE Collaboration's recent measurements provide a dependence of charged hadron cumulant ratios on the collision energy per nucleon-nucleon pair $\sqrt{s_{NN}}$ between 5.1 and 17.3 GeV for different colliding systems (p+p, Be+Be, and Ar+Sc) [62, 63]. However, no indication of critical behavior is observed. The same conclusion is also drawn from the analysis of the scaled factorial moments in central Ar+Sc and Pb+Pb collisions [24, 62].

The results of the STAR and HADES Collaborations [52, 58] suggest that the proton and net-proton number cumulant ratio κ_4/κ_2 measured in central (0-5%) Au+Au collisions does depend non-monotonically on the collision energy, see Fig. 2.3.[5] Note that the experimental uncertainties especially at the lower energies are still quite large. Therefore, greater statistics are needed.

[5]Note that the HADES data point and the STAR measurement at $\sqrt{s_{NN}} = 3$ GeV are obtained in different acceptance which makes the comparison challenging as discussed, e.g., in my recent paper [64].

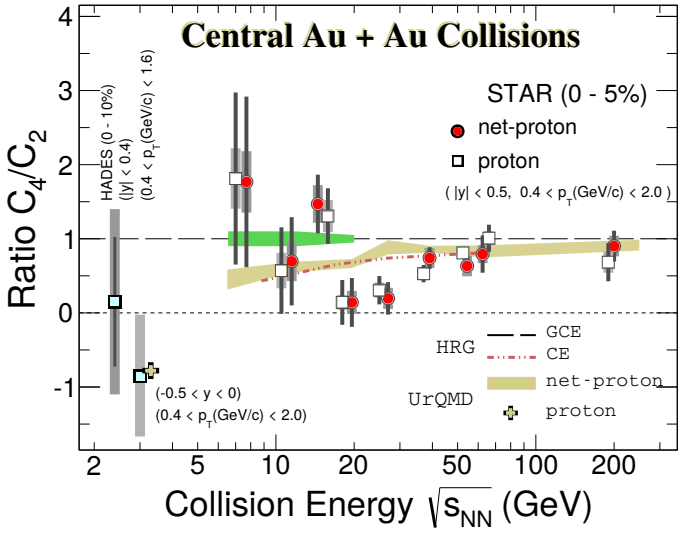

Figure 2.3: The proton and net-proton cumulant ratio κ_4/κ_2 (denoted by STAR as C_4/C_2) measured by the STAR Collaboration (plus one data point from the HADES Collaboration) in central (0-5%) Au+Au collisions [52, 58]. Data points are compared with model predictions. Note that the HADES data point and the STAR measurement at $\sqrt{s_{NN}} = 3$ GeV are obtained in different acceptance.

These results might be interpreted as a possible signature of the desired critical phenomena. However, one should be careful because the fluctuations may be caused by other non-critical contributing effects. They play the role of background in the search for the signal of phase transition and critical point.

One important example of such background effects is known as volume fluctuation [65]. The impact parameter in the atomic nuclei collision, thus the resulting overlapping geometry, and the number of wounded nucleons[6] fluctuate event by event. It is impossible to measure directly the initial geometry of a collision. Instead, the collision centrality is determined based on the number of produced particles which is related to the number of participants and can be studied using the Monte Carlo simulations based on the Glauber model [66–71]. Even the tight centrality cuts do not fully reduce the volume fluctuations. Nowadays, in experimental data analysis, centrality bin width correction (CBWC) [72] is used to address this issue [22]. In some analyses, it is convenient to use strongly intensive quantities [73–75].

Another contribution to baryon number fluctuations originates from the global baryon number conservation law [76]. The baryons are always produced as baryon-antibaryon pairs and can annihilate also as such pairs. Therefore, the total net-baryon number is conserved. If all the particles were observed, the baryon number would not fluctuate in the experimental results. This corresponds to the canonical ensemble known in statistical mechanics. If the measurable part was much smaller than the total system, it would be described by the grand canonical ensemble in which the number of particles is not fixed since the system can exchange them with the reservoir. Real experiments represent a case between these two extreme scenarios since a finite acceptance is covered by the detectors. The baryon number fluctuates because a particle can be inside or

[6] A wounded nucleon (a.k.a. participating nucleon) is a nucleon of an incoming nucleus that underwent at least one inelastic collision with a nucleon from another nucleus.

outside the acceptance but the system (inside the acceptance) is comparable in size to the reservoir (outside the acceptance). In Ref. [76] it was shown that the global baryon number conservation law significantly modifies the baryon number cumulants. Many recent studies are taking this effect into account, e.g., Refs. [77–79].

The ALICE Collaboration measured the normalized second net-proton cumulant

$$R_1 = \frac{\kappa_2(n_p - n_{\bar{p}})}{\langle n_p + n_{\bar{p}} \rangle} \tag{2.40}$$

as a function of the pseudorapidity[7] interval size in central (0-5%) Pb+Pb collisions at $\sqrt{s_{NN}} = 2.76$ TeV, see Fig. 2.4 [80]. They showed that in the interpretation of these results, the global baryon number conservation is favored over local conservation and it leads to long-range correlations. Recently, in Ref. [81], another explanation was proposed. The local baryon conservation underestimates data however baryon-antibaryon annihilation results in a decrease of the denominator of R_1 while keeping its numerator unchanged. Therefore, the combination of the baryon-antibaryon annihilation and local baryon number conservation may also reproduce the ALICE data. Further measurements of other cumulants and factorial cumulants are necessary to distinguish between the two scenarios.

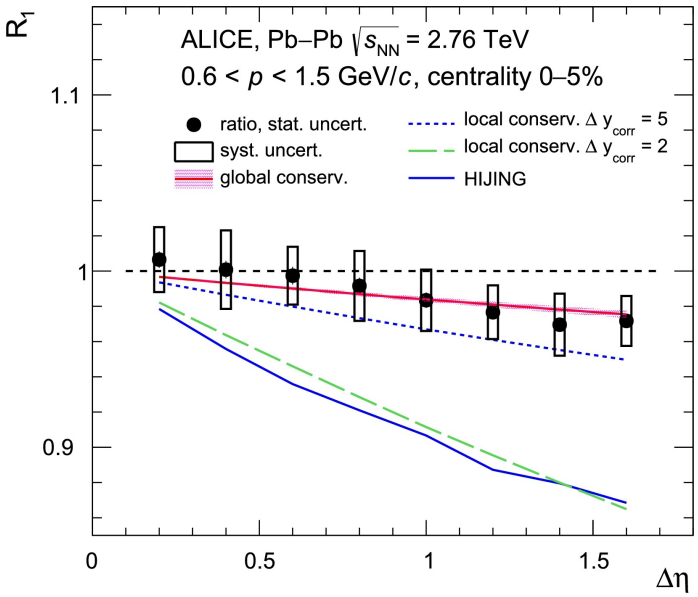

Figure 2.4: The normalized second net-proton cumulant, $R_1 = \kappa_2(n_p - n_{\bar{p}})/\langle n_p + n_{\bar{p}} \rangle$, as a function of the pseudorapidity interval size, $\Delta\eta$, measured by the ALICE Collaboration in central (0-5%) Pb+Pb collisions at $\sqrt{s_{NN}} = 2.76$ TeV, compared with different models [80].

In heavy-ion collision experiments, the particles are observed by the detector systems only in some regions of the momentum space. This fact is often modeled by the binomial acceptance in which each produced particle has the same probability of being observed. In Ref. [78], the subensemble acceptance method (SAM) was proposed instead. In this method, the system is divided into two subsystems. All the

[7] The pseudorapidity is defined as $\eta = -\ln\left(\tan\left(\frac{\theta}{2}\right)\right)$, where θ is the angle between the momentum of a particle and the beam axis (the axis along which the incoming nuclei are moving).

particles from the first subsystem are observed whereas all the others are not. The partition function is given by [78, 82]

$$Z(V,T) = \sum_N Z_{CE}(V,N,T) Z_{CE}(V_0 - V, N_0 - N, T)\,, \tag{2.41}$$

where Z_{CE} is the canonical ensemble partition function, V and $V_0 - V$ are the volumes of the subsystems, N and $N_0 - N$ are the numbers of particles in the subsystems, and T is a common temperature of two systems being in thermal equilibrium with each other.[8] Authors have derived the net-baryon cumulants with baryon number conservation in terms of cumulants without baryon number conservation within SAM. This method has already been applied in a couple of studies to correct the results for the baryon number conservation, see, e.g., Refs. [79, 82, 83].

2.4 The goal of this thesis

In this introduction, some unanswered questions about the QCD phase diagram arose. Further theoretical predictions as well as more experimental data on the cumulants and factorial cumulants of the conserved charges are needed in the search for the first-order phase transition and the corresponding critical point between hadronic matter and quark-gluon plasma. Undoubtedly, a better understanding of how different effects influence the quantities measured experimentally in heavy-ion collisions is necessary. This may be also useful in the studies of the initial conditions and properties of strongly interacting matter in heavy-ion collisions.

The goal of my research was to contribute to these efforts by calculating the cumulants and factorial cumulants originating from the various effects which are important when exploring the QCD phase diagram. These effects included global baryon number conservation, short-range correlations, and longitudinal fluctuations of fireball density.

[8] Clearly, V_0 is the total volume and N_0 is the total particle number in the two subsystems. It is assumed that the two subsystems do not interact with each other which can be approximately the case for very short-range correlations between particles.

Chapter 3

Summary of the articles

The core of this doctoral thesis consists of four published articles. In all the articles, the proton or baryon number cumulants and factorial cumulants originating from different phenomena are calculated. These effects are important in the search for the predicted first-order phase transition and the critical point in the QCD phase diagram. The studies are based on fully analytical calculations which I believe is worth noting.

The mixed proton-antiproton factorial cumulants from the global baryon number conservation are calculated in Article 1. In Article 2, the baryon number cumulants and factorial cumulants are extracted assuming global baryon number conservation and short-range correlations. In Article 3, a new method based on the previous paper is developed to achieve more precise results, especially for small systems. In Article 4, the approach to obtain the proton number cumulants and factorial cumulants due to the fluctuations in the width of the proton rapidity density distribution is proposed. These fluctuations are expected to appear because of the fireball density longitudinal fluctuations.

My contribution to all these articles was to plan and perform all the calculations using, among others, the Mathematica software [84]. I also prepared the plots using Matplotlib, the package for creating visualizations in Python [85]. I wrote the first drafts of all the published articles. Also, I actively participated in discussions on the subsequent steps of each research project and on the interpretation of the results.

In the summary of the articles, I refer to sections, figures, and equations from the articles by their numbers. To avoid ambiguity, the equations, and figures from the main text of the thesis are referred to by a number preceded by a number of a section.

3.1 Article 1

M. Barej and A. Bzdak, *Factorial cumulants from global baryon number conservation*, Phys. Rev. C 102, no. 6, 064908 (2020).

The aim of Article 1 [86] was to calculate analytically the proton, antiproton, and mixed proton-antiproton factorial cumulants of different orders assuming that the global baryon number conservation is the only source of correlations in relativistic heavy-ion collisions. As explained in the previous section, the baryon number conservation is an important background effect in the search for critical fluctuations. Hence, it needs better understanding and theoretical predictions. The main findings of this article include the factorial cumulant generating function from global baryon number conservation, exact formulas for the corresponding factorial cumulants, and simple relations between them. Approximations for net-baryon number $B = 0$ are provided and it is shown that they work very well.

As mentioned earlier, the ALICE Collaboration results on the normalized second net-proton cumulant obtained in central Pb+Pb collisions at $\sqrt{s_{NN}} = 2.76$ TeV [80] can be explained by the global baryon number conservation law. To confirm this interpretation and distinguish it from another explanation that assumes baryon-antibaryon annihilation and local baryon number conservation suggested in Ref. [81], it would be helpful to measure mixed factorial cumulants or other cumulants and compare them with the predictions presented in this paper.

The starting point of the calculation is the probability distribution of observing n_p protons and $\bar{n}_p$ antiprotons,

$$\begin{aligned} P(n_p,\bar{n}_p) =& A\sum_{N_b=n_p}^{\infty}\sum_{\bar{N}_b=\bar{n}_p}^{\infty}\delta_{N_b-\bar{N}_b,B}\left[\frac{\langle N_b\rangle^{N_b}}{N_b!}e^{-\langle N_b\rangle}\right]\left[\frac{\langle \bar{N}_b\rangle^{\bar{N}_b}}{\bar{N}_b!}e^{-\langle \bar{N}_b\rangle}\right] \\ &\times\left[\frac{N_b!}{n_p!(N_b-n_p)!}p^{n_p}(1-p)^{N_b-n_p}\right]\left[\frac{\bar{N}_b!}{\bar{n}_p!(\bar{N}_b-\bar{n}_p)!}\bar{p}^{\bar{n}_p}(1-\bar{p})^{\bar{N}_b-\bar{n}_p}\right], \end{aligned} \tag{3.1}$$

where the baryon number, N_b, and antibaryon number, $\bar{N}_b$, follow the Poisson distribution. The binomial acceptance with probability p that a baryon is observed as a proton, and $\bar{p}$ that an antibaryon is observed as an antiproton, does not provide any correlations. The global baryon number conservation is required by the Kronecker delta where B is the net-baryon number. A is a normalization constant. Therefore, the global baryon number conservation is the only source of correlations in this model.

Using this probability distribution, the bivariate factorial cumulant generating function, $G(x,\bar{x})$, see Eq. (5), is obtained,

$$G(x,\bar{x}) = \ln\left[\left(\frac{px+1-p}{\bar{p}\bar{x}+1-\bar{p}}\right)^{\frac{B}{2}}\frac{I_B\left(2\sqrt{\langle N_b\rangle\langle\bar{N}_b\rangle(px+1-p)(\bar{p}\bar{x}+1-\bar{p})}\right)}{I_B\left(2\sqrt{\langle N_b\rangle\langle\bar{N}_b\rangle}\right)}\right], \tag{3.2}$$

where $I_n(x)$ is a modified Bessel function of the first kind. Using this generating function, the mixed factorial cumulants, $\hat{C}^{(n,m)}$, for n protons and m antiprotons are calculated. The exact formulas are given by Eqs. (14)-(28). They are expressed in terms of the variables introduced to simplify the formulas. Nevertheless, all these variables depend on B and $z = \sqrt{\langle N_b\rangle\langle\bar{N}_b\rangle}$ only. Clearly, these mixed factorial cumulants carry more

information than net-proton cumulants. In particular, a proton–antiproton factorial cumulant, $\hat{C}^{(1,1)}$, can be useful. It is emphasized that $\hat{C}^{(n,m)}$ can be obtained experimentally using the measurement of the factorial moments of two variables, as shown in Appendix D. The net-proton cumulants can be calculated from the mixed factorial cumulants as presented in Appendix C. This enables a comparison with many experimental results.

In Section III B, it is noted that $\hat{C}^{(n,m)}$'s are proportional to $p^n\bar{p}^m$. Therefore, it was natural to define the acceptance-independent quantity $\hat{R}^{(n,m)} = \hat{C}^{(n,m)}/(p^n\bar{p}^m)$. Simple relations between $\hat{R}^{(n,m)}$'s are given in Eqs. (32)-(40), and summarized in Eq. (41). In Section III C, approximate formulas for the special case of $B = 0$ that corresponds to large collision energies are provided, see Eqs. (44)-(57). They are obtained from the asymptotic expansion of the Bessel function. It is shown that $\hat{R}^{(n,m)}$ is approximately proportional to the mean baryon number with baryon number conservation, $\langle N_b\rangle_c$. In Section IV A, the comparison with exact results shows that this approximation works very well and also that $\hat{R}^{(n,m)}$ is proportional to $\langle N_b\rangle_c$ already at quite small $\langle N_b\rangle_c$. In Section IV B, the exact results for an example of the finite $B = 300$ that corresponds to lower collision energies are presented.

3.2 Article 2

M. Barej and A. Bzdak, *Factorial cumulants from short-range correlations and global baryon number conservation*, Phys. Rev. C 106, no. 2, 024904 (2022).

The aim of Article 2 [87] was to calculate analytically the baryon number factorial cumulants and cumulants of different orders with arbitrary short-range correlations. The global baryon number conservation is assumed to be the only source of long-range correlations. The cumulants are obtained in a subsystem. This follows the idea of the subensemble acceptance method (SAM) [78], discussed in the previous section. This research is another step towards better understanding the influence of the baryon number conservation on the baryon number correlations and fluctuations. The key result of this article is the analytic factorial cumulant generating function from global baryon number conservation with short-range correlations. The corresponding cumulants and factorial cumulants are presented. It is found that in the limit of large baryon number, B, the mth factorial cumulant in the subsystem with baryon conservation is dominated by k-particle short-range correlations where $k \leq m$. The cumulants with baryon conservation and short-range correlations are expressed by the global, short-range cumulants without baryon conservation. These relations reproduce the findings of Ref. [78] but are obtained in a different way.

A system produced in a heavy-ion collision is considered. It is divided into two subsystems, say inside and outside the acceptance. The probability that there are n_1 baryons in the first subsystem (inside the acceptance) and n_2 baryons in the second subsystem (outside the acceptance) is given by

$$P_B(n_1, n_2) = A\ P_1(n_1)P_2(n_2)\delta_{n_1+n_2,B}\,, \tag{3.3}$$

where P_1 and P_2 are the probability multiplicity distributions without baryon number conservation in the first and second subsystem, respectively. P_1 and P_2 include only short-range correlations which are modeled by the corresponding factorial cumulants, $\hat{C}^{(i)}_k = \langle n_i\rangle\alpha_k$, $i = 1, 2$, being proportional to the mean number of

baryons in the ith subsystem, $\langle n_i \rangle$. α_k is interpreted as a k-particle short-range correlation strength, common in the whole system. A is a normalization constant, and the global baryon number conservation is required by the Kronecker delta with B being the total conserved baryon number in the system. For simplicity, in this study, only baryons are considered and antibaryons are neglected. This applies to low collision energies in which very few antibaryons are created.

The probability that there are n_1 baryons inside the acceptance, assuming baryon number conservation and short-range correlations, is obtained by summing Eq. (3.3) over n_2, see Eq. (3). The next step is to calculate the corresponding factorial cumulant generating function, $G_{(1,B)}(z)$, see Eq. (9). Using the integral representation of the Kronecker delta and Cauchy's differential formula, one obtains

$$G_{(1,B)}(z) = \ln \left[\frac{A}{B!} \frac{d^B}{dx^B} \exp \left(\sum_{k=1}^{\infty} \frac{(xz-1)^k \hat{C}_k^{(1)} + (x-1)^k \hat{C}_k^{(2)}}{k!} \right) \Bigg|_{x=0} \right] . \tag{3.4}$$

Note that this expression includes the Bth derivative where B can be greater than 300. Using Faà di Bruno's formula, this equation can be rewritten in terms of the complete exponential Bell polynomials, see Eq. (14). Eventually, the factorial cumulants in the first subsystem with global baryon number conservation and short-range correlations are calculated by differentiating the generating function, $\hat{C}_k^{(1,B)} = \frac{d^k}{dz^k} G_{(1,B)}(z) \Big|_{z=1}$.

First, this formalism is applied to the simple case where only two-particle short-range correlations are considered, i.e., $\alpha_k = 0$ for $k > 2$. Consequently, $\hat{C}_k^{(1)} = \hat{C}_k^{(2)} = 0$ for $k > 2$. An analytic approach leads to the finite generating function, see Section III A. An approximate method using the general Leibnitz formula and assuming a small α_2 is shown in Section III B. The results are illustrated by plots in Fig. 2. They show that for quite large $B = 300$ and 20% acceptance (denoted by $f = 0.2$), the second and third factorial cumulants, $\hat{C}_2^{(1,B)}$ and $\hat{C}_3^{(1,B)}$, are very well described by the linear function of α_2. This is also supported by Eqs. (34)-(35). The higher-order factorial cumulants, $\hat{C}_4^{(1,B)}$, $\hat{C}_5^{(1,B)}$, and $\hat{C}_6^{(1,B)}$, are well approximated by the quartic expansion.

In Section IV, the approximate approach (for small α_k) is applied to the case of the multiparticle short-range correlations. It is found that in the limit of large B, the nth factorial cumulant in the first subsystem with baryon number conservation, $\hat{C}_n^{(1,B)}$, is weakly influenced by α_k with $k > n$. For instance, in $\hat{C}_3^{(1,B)}$, only α_2 and α_3 (corresponding to two- and three-particle short-range correlations) are significant, whereas terms with α_4, α_5, etc. are suppressed.

The cumulants can be calculated from the factorial cumulants, see Eq. (2.24). In Section V, it is shown that our results in the limit of small α_k and large B reproduce the findings of Ref. [78] that were obtained in a different way, using statistical mechanics. The cumulants with baryon number conservation are expressed in terms of the global cumulants (in the whole system) without baryon number conservation, $\kappa_m^{(G)}$, where both kinds of cumulants allow for short-range correlations. $\kappa_m^{(G)}$ is obtained from the short-range global factorial cumulants, $\hat{C}_n^{(G)} = B\alpha_n$, where the total average number of baryons $\langle N \rangle = B$. The relations between cumulants with and without baryon number conservation make it possible to compensate the experimental data and Lattice QCD results for the contribution from this conservation law.

3.3 Article 3

M. Barej and A. Bzdak, *Cumulants from short-range correlations and baryon number conservation at next-to-leading order*, Phys. Rev. C 107, no. 3, 034914 (2023).

The aim of Article 3 [88] was to calculate the first correction to earlier obtained baryon number cumulants in the subsystem from global baryon number conservation and short-range correlations. Previously, these cumulants were obtained within the limit of a large baryon number, B. However, for small systems such as Be+Be or Ar+Sc studied experimentally by the NA61/SHINE Collaboration or for peripheral collisions of larger systems, it is important to provide a more precise result that is valid also at smaller B. The main findings of this article are the simple analytic expressions for the leading-order and next-to-leding-order terms of the studied cumulants. They depend only on the size of the subsystem (expressed by a fraction of the total system) and on the short-range cumulants without baryon number conservation. It is checked that the next-to-leading-order term improves the results, in particular for small B. It is also pointed out that the multiparticle short-range correlation strengths cannot be completely arbitrary but are subjected to constraints coming from the probability theory.

The study from the previous paper [87] is extended in this article, by proposing a method of calculating higher-order terms of the expansion of a cumulant. The factorial cumulant generating function (3.4) is approximated by Eq. (6), where α_k's are assumed to be small. Then, the general Leibnitz formula is used to obtain a useful form of the factorial cumulant generating function and the factorial cumulants. The cumulants are calculated from the factorial cumulants by Eq. (2.24).

These cumulants in the subsystem with baryon number conservation and short-range correlations, $\kappa_n^{(1,B)}$, are expanded into power series in terms of B:

$$\kappa_n^{(1,B)} \approx \underbrace{\kappa_n^{(1,B,\mathrm{LO})}}_{u_{n,1}B^1} + \underbrace{\kappa_n^{(1,B,\mathrm{NLO})}}_{u_{n,0}B^0} + \underbrace{\ldots}_{O(B^{-1})} , \tag{3.5}$$

where $\kappa_n^{(1,B,\mathrm{LO})}$ and $\kappa_n^{(1,B,\mathrm{NLO})}$ are the leading-order and next-to-leading-order terms of the power series in B, respectively. The leading-order term is linear in B, the next-to-leading-order term is independent of B, and higher-order corrections are proportional to subsequent negative powers of B. $\kappa_n^{(1,B,\mathrm{LO})}$'s have already been obtained in the previous paper [87] and agree with the results of Ref. [78] that were derived in the thermodynamic limit. Our method allows us to obtain also next-to-leading-order terms and, in principle, also higher-order terms. Eqs. (14) and (17) present a method of extracting the leading-order, next-to-leading-order, and even higher-order terms, by analogy.

The main results, i.e., the leading-order and next-to-leading-order terms are presented in Section III, Eqs. (19)-(25). The cumulants in the subsystem with baryon number conservation, $\kappa_n^{(1,B)} \approx \kappa_n^{(1,B,\mathrm{LO})} + \kappa_n^{(1,B,\mathrm{NLO})} + \ldots$, are expressed by the global, short-range cumulants without baryon conservation, $\kappa_n^{(G)}$, and

a fraction of the baryons in the subsystem, f. For example, the first two terms of the fourth cumulant read

$$\begin{aligned}\kappa_4^{(1,B,\mathrm{LO})} &= f\bar{f}\left[\kappa_4^{(G)} - 3f\bar{f}\left(\kappa_4^{(G)} + \frac{(\kappa_3^{(G)})^2}{\kappa_2^{(G)}}\right)\right], \\ \kappa_4^{(1,B,\mathrm{NLO})} &= \frac{1}{2}f\bar{f}\left\{\frac{\kappa_3^{(G)}\kappa_5^{(G)} - \kappa_2^{(G)}\kappa_6^{(G)}}{(\kappa_2^{(G)})^2}\right. \\ &\left. + 3f\bar{f}\left[\frac{2(\kappa_3^{(G)})^4 - 5\kappa_2^{(G)}(\kappa_3^{(G)})^2\kappa_4^{(G)} + (\kappa_2^{(G)})^2\kappa_3^{(G)}\kappa_5^{(G)}}{(\kappa_2^{(G)})^4} + \frac{(\kappa_4^{(G)})^2 + \kappa_2^{(G)}\kappa_6^{(G)}}{(\kappa_2^{(G)})^2}\right]\right\},\end{aligned} \tag{3.6}$$

where $\bar{f} = 1 - f$.

The next-to-leading-order terms are sufficient to obtain a very good precision as seen from the example in Section IV, Fig. 2., where the leading-order and leading- plus next-to-leading-order approximations are compared with the exact results following from the direct, brute force calculations. It is seen that the next-to-leading-order term improves the results. It has also been checked that this conclusion remains true for other choices of α_k and f parameters. However, it is worth noticing that the values of α_k's cannot be arbitrary. As presented in Appendix B, the multiplicity probability distribution can be written as (Eq. (B1))

$$P(m) = \frac{1}{m!}\frac{d^m}{dz^m}\left[\exp\left(\sum_{k=1}^{\infty}\frac{(z-1)^k}{k!}\hat{C}_k\right)\right]\Bigg|_{z=0}, \tag{3.7}$$

where $\hat{C}_k = B\alpha_k$. Obviously, $P(m)$ for any $0 \leq m \leq B$ has to satisfy the condition $0 \leq P(m) \leq 1$. Also, the even central moments, $\mu_k = \langle(m - \langle m\rangle)^k\rangle$ (with k - even), have to be greater than or equal to 0. The inequality between kurtosis, μ_4/σ^4, and skewness, S, $\frac{\mu_4}{\sigma^4} \geq S^2 + 1$ [89] results in relations between α_k's as well.

Appendix A presents an alternative approach to finding the $\kappa_n^{(1,B,\mathrm{LO})}$ and $\kappa_n^{(1,B,\mathrm{NLO})}$ terms. This method uses the series expansion.

3.4 Article 4

M. Barej and A. Bzdak, *Cumulants from fluctuating width of rapidity distribution*, Phys. Rev. C 108, no. 1, 014907 (2023).

The aim of Article 4 [64] was to study the correlations originating from the fluctuations in the width of the proton rapidity density distribution. The multiparticle rapidity correlation functions, factorial cumulants, and cumulants due to this effect are calculated analytically. The most important findings include the fact that for small fluctuations in the width of the rapidity distribution, the proton number cumulant ratios are independent of the width distribution and are dominated by two-particle correlations. Importantly, the cumulant ratios are of the same order as those measured by the STAR Collaboration. Hence, this effect should be taken into account when discussing proton number cumulants. It is also demonstrated that the size of the rapidity interval strongly influences the cumulant ratios.

The fluctuations in the width of the proton rapidity density distribution can arise for instance from the longitudinal fluctuations of the fireball density. In particular, in low-energy collisions, some of the protons

and neutrons from the incoming nuclei are stopped close to the interaction region. The corresponding energy deposition due to baryon stopping fluctuates event by event and results in the longitudinal fluctuations of the density of the created fireball. These fluctuations affect the way how the particles are emitted in the longitudinal direction and may result in changes in the width of the proton rapidity density distribution measured experimentally. So far, the longitudinal fluctuations have been studied by expanding the rapidity multiplicity distribution into orthogonal polynomials [90]. This idea has been further investigated theoretically and experimentally, see, e.g., Refs. [56, 91–95]. The new approach proposed in this article focuses on the fluctuations in the width of the distribution.

In central Au+Au collisions at low energies, the proton rapidity density distribution, $dN/dy = \varrho(y)$, can be well described by the Gaussian function. In the midrapidity region ($y \approx 0$), it can be approximated by the quadratic function [96],

$$\varrho(y) \approx \frac{N_t}{\sqrt{2\pi}\sigma} \exp\left(-\frac{y^2}{2\sigma^2}\right) \approx \frac{N_t}{\sqrt{2\pi}\sigma}\left(1 - \frac{y^2}{2\sigma^2}\right) , \tag{3.8}$$

where $N_t = \int_{-\infty}^{+\infty} dy \varrho(y)$ is the total number of protons; see Eqs. (1) and (2).[1] The fact that the width of this distribution fluctuates event by event can be modeled by the assumption that the standard deviation, σ, is itself a random variable following a probability distribution $p(\sigma)$. Thus, the rapidity density distribution for a given σ will be denoted by $\varrho(y, \sigma)$. The measured single-proton rapidity distribution is averaged over many events (over σ), see Eq. (4),

$$\varrho_{\text{meas}}(y) = \int d\sigma \varrho(y, \sigma) p(\sigma) . \tag{3.9}$$

Similarly, the averaged two-particle rapidity distribution is given by, see Eq. (5),

$$\varrho_{\text{meas,2}}(y_1, y_2) = \int d\sigma \varrho(y_1, \sigma) \varrho(y_2, \sigma) p(\sigma) . \tag{3.10}$$

Then, the corresponding two-particle rapidity correlation function reads, see Eq. (6),

$$C_2(y_1, y_2) = \varrho_{\text{meas,2}}(y_1, y_2) - \varrho_{\text{meas}}(y_1)\varrho_{\text{meas}}(y_2) , \tag{3.11}$$

and the second factorial cumulant is obtained by, see Eq. (7),

$$\hat{C}_2 = \int_{-Y}^{Y} dy_1 dy_2 \, C_2(y_1, y_2) , \tag{3.12}$$

where Y characterizes the rapidity interval in which the measurement or calculation is carried. The higher-order factorials cumulants are obtained analogously from the multiparticle correlation functions defined, e.g., in Ref. [56], see Eqs. (8)-(10) of Article 4.

Then, this formalism is applied to the quadratic rapidity distribution (3.8). The multiparticle correlation functions and the corresponding factorial cumulants are expressed in terms of N_t, Y, and $m_k = \langle 1/\sigma^k \rangle = \int d\sigma \, \frac{p(\sigma)}{\sigma^k}$, see Eqs. (12)-(25) and (A1)-(A8).

The underlying $p(\sigma)$ distribution is unknown. Therefore, three qualitatively different probability distributions, the uniform, triangular, and lognormal distributions, have been tried. Obviously, there are many

[1] For higher collision energies, already slightly below 10 GeV, a bimodal structure of the proton rapidity density distribution becomes visible. However, the goal of the study is to explore the effect and provide a rough estimation rather than precise results.

other possible choices but I believe these three are a representative selection to investigate the effect. The three distributions are required to have the same mean and variance so that the results can be compared. The m_k's can be used to obtain exact results. Much simpler, approximated formulas for the factorial cumulants are given in Section II B.

The cumulants and the cumulant ratios are calculated from the factorial cumulants. In Section III A, those ratios are plotted, assuming the values of the parameters that roughly correspond to proton rapidity distribution from central Au+Au collisions at $\sqrt{s_{NN}} = 7.7$ GeV. For small fluctuations in the width of the proton rapidity distribution, the cumulant ratios obtained with all three $p(\sigma)$ give very similar results as seen in Fig. 3.1. Indeed, the expansion in Eq. (49) shows that the two leading terms are independent of $p(\sigma)$. Moreover, it turns out that these small fluctuations in width are governed by two-particle correlations.

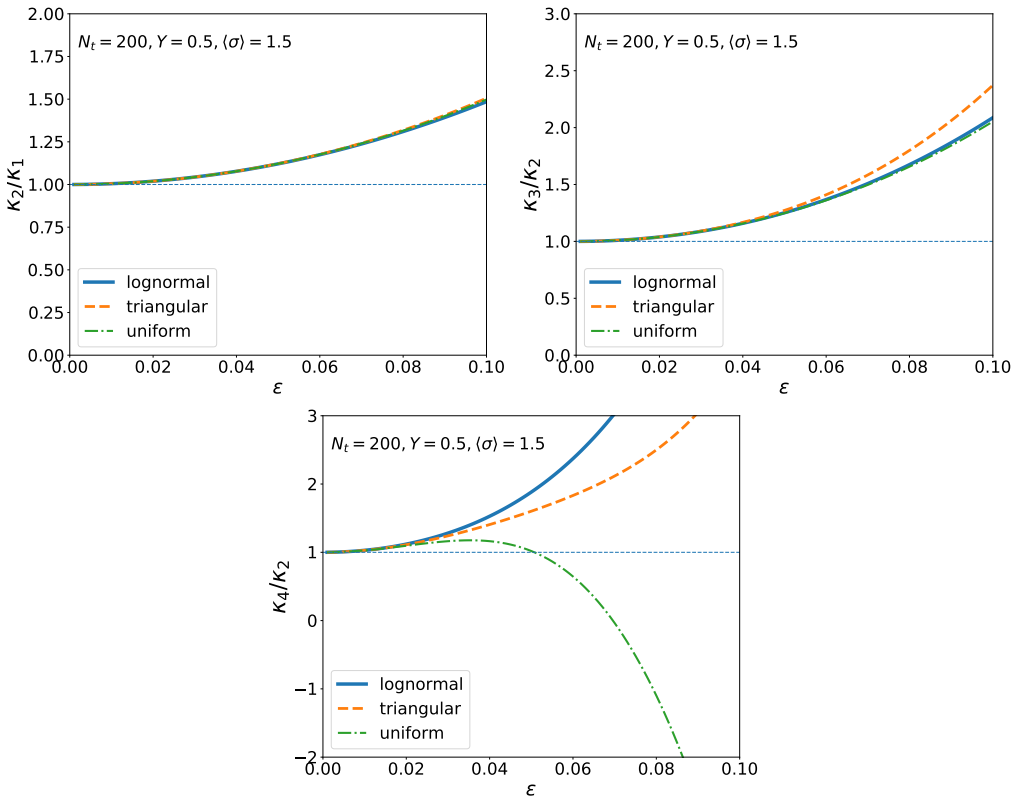

Figure 3.1: The cumulant ratios from the fluctuations in width of the quadratic proton rapidity distribution with different underlying $p(\sigma)$. ε determines the strength of width fluctuations and is defined by $\sqrt{\langle(\sigma - \langle\sigma\rangle)^2\rangle} = \varepsilon\langle\sigma\rangle$.

In Figs. 4 and 5, the approximated results are compared with the exact ones. In Fig. 6, the cumulant ratios calculated numerically for the truncated normal distribution are shown.

In Section III B, it is demonstrated how the cumulants and factorial cumulants are modified when the rapidity interval size changes. In particular, the symmetric interval ($|y| < 0.5$) and two times shorter asymmetric interval ($-0.5 < y < 0$), which correspond to different measurements by the STAR Collaboration [52], are discussed. The cumulant ratios differ significantly when obtained within these two rapidity intervals.

Finally, it is noted that the cumulant ratios due to the fluctuations in width are of the same order of magnitude as those measured by the STAR Collaboration [59]. Therefore, this effect should be taken into account when studying the proton number cumulants in the search for the QCD first-order phase transition and related critical endpoint.

Chapter 4

Summary

In this set of articles, the mathematical models of various effects present in relativistic heavy-ion collisions have been introduced and investigated. The proton and baryon number cumulants and factorial cumulants have been calculated analytically. These results may be important in the ongoing search for the expected phase transition and critical endpoint between the hadron gas and quark-gluon plasma.

The mixed proton-antiproton factorial cumulants from the global baryon number conservation law have been obtained for the first time. They carry more information than often studied net-proton cumulants and, when measured, may shed light on the distinction between the effects of global and local baryon number conservation. They might be also helpful in studying non-trivial multiparticle correlations in the relativistic collisions of atomic nuclei. The acceptance-independent observable has been suggested. The special cases of small and large net-baryon numbers have been discussed.

The original approach to calculating the cumulants and factorial cumulants in the subsystem resulting from the global baryon number conservation and short-range correlations has been presented. It is assumed that antibaryons can be neglected. This applies to low collision energies. It has been demonstrated that for the mth factorial cumulant, the short-range correlations of more than m particles are suppressed at large baryon numbers. With this method, it has also been possible to reproduce the relations obtained using statistical mechanics with the subensemble acceptance method. Namely, the cumulants subject to baryon number conservation and short-range correlations have been related to the global short-range cumulants without baryon number conservation. This enables extracting the influence of this conservation law.

Afterward, a method of obtaining more precise results expressed by the next-to-leading-order terms of the cumulant expansions has been proposed. These terms are also expressed by the global short-range cumulants without baryon conservation. This correction is needed especially for the small colliding systems, e.g., Ar+Sc or Be+Be studied in the experiments by the NA61/SHINE Collaboration at the CERN SPS or even in the peripheral collisions of large nuclei. The limitations of the short-range correlation strengths originating from the probability theory have also been discussed.

In the latest research, a new method of studying the longitudinal fluctuations of the fireball density has been proposed. This effect likely leads to fluctuations in the width of the proton rapidity density distribution. It has been explained how to calculate the cumulants and factorial cumulants due to these fluctuations. It has been observed that for small fluctuations in width, the cumulant ratios are independent of the underlying

distribution of width and that they are controlled by two-particle correlations. Then, it has been demonstrated that the cumulant ratios strongly depend on the rapidity interval size. The results have been presented in the context of the STAR Collaboration measurements. The comparison suggests that the effect of fluctuations in the width of the proton rapidity distribution may be significant and more attention should be drawn to it.

Bibliography

[1] A. Bzdak, S. Esumi, V. Koch, J. Liao, M. Stephanov, and N. Xu, "Mapping the Phases of Quantum Chromodynamics with Beam Energy Scan," *Phys. Rept.*, vol. 853, pp. 1–87, 2020.

[2] A. Aprahamian *et al.*, "Reaching for the horizon: The 2015 long range plan for nuclear science," 10 2015. `https://www.osti.gov/biblio/1296778`, Accessed: 02-05-2023.

[3] D. Tong, *Statistical Physics*. 2012. `http://www.damtp.cam.ac.uk/user/tong/statphys.html`, Accessed: 02-05-2023.

[4] J.-Y. Ollitrault, "Anisotropy as a signature of transverse collective flow," *Phys. Rev. D*, vol. 46, pp. 229–245, 1992.

[5] (STAR), Ackermann, K. H., *et al.*, "Elliptic flow in Au + Au collisions at (S(NN))**(1/2) = 130 GeV," *Phys. Rev. Lett.*, vol. 86, pp. 402–407, 2001.

[6] (PHENIX), K. Adcox, *et al.*, "Suppression of hadrons with large transverse momentum in central Au+Au collisions at $\sqrt{s_{NN}}$ = 130-GeV," *Phys. Rev. Lett.*, vol. 88, p. 022301, 2002.

[7] (PHENIX), S. S. Adler, *et al.*, "High transverse momentum η meson production in p^+p, d^+ Au and Au+Au collisions at $S(NN)^{(1/2)}$ = 200-GeV," *Phys. Rev. C*, vol. 75, p. 024909, 2007.

[8] J. Rafelski and B. Muller, "Strangeness Production in the Quark - Gluon Plasma," *Phys. Rev. Lett.*, vol. 48, p. 1066, 1982. [Erratum: Phys.Rev.Lett. 56, 2334 (1986)].

[9] P. Koch, B. Muller, and J. Rafelski, "Strangeness in Relativistic Heavy Ion Collisions," *Phys. Rept.*, vol. 142, pp. 167–262, 1986.

[10] C. Blume and C. Markert, "Strange hadron production in heavy ion collisions from SPS to RHIC," *Prog. Part. Nucl. Phys.*, vol. 66, pp. 834–879, 2011.

[11] M. G. Alford, A. Schmitt, K. Rajagopal, and T. Schäfer, "Color superconductivity in dense quark matter," *Rev. Mod. Phys.*, vol. 80, pp. 1455–1515, 2008.

[12] K. Rajagopal and F. Wilczek, *The Condensed matter physics of QCD*, pp. 2061–2151. 11 2000. in: M. Shifman, and B. Ioffe, *At the frontier of particle physics. Handbook of QCD. Vol. 1-3*.

[13] P. Braun-Munzinger and J. Wambach, "The Phase Diagram of Strongly-Interacting Matter," *Rev. Mod. Phys.*, vol. 81, pp. 1031–1050, 2009.

[14] Y. Aoki, G. Endrodi, Z. Fodor, S. D. Katz, and K. K. Szabo, "The Order of the quantum chromodynamics transition predicted by the standard model of particle physics," *Nature*, vol. 443, pp. 675–678, 2006.

[15] A. Bazavov *et al.*, "Equation of state and QCD transition at finite temperature," *Phys. Rev. D*, vol. 80, p. 014504, 2009.

[16] G. Aarts, "Introductory lectures on lattice QCD at nonzero baryon number," *J. Phys. Conf. Ser.*, vol. 706, no. 2, p. 022004, 2016.

[17] M. A. Stephanov, "QCD phase diagram and the critical point," *Prog. Theor. Phys. Suppl.*, vol. 153, pp. 139–156, 2004.

[18] M. A. Stephanov, "QCD phase diagram: An Overview," *PoS*, vol. LAT2006, p. 024, 2006.

[19] P. Braun-Munzinger, V. Koch, T. Schäfer, and J. Stachel, "Properties of hot and dense matter from relativistic heavy ion collisions," *Phys. Rept.*, vol. 621, pp. 76–126, 2016.

[20] A. Chodos, R. L. Jaffe, K. Johnson, C. B. Thorn, and V. F. Weisskopf, "A New Extended Model of Hadrons," *Phys. Rev. D*, vol. 9, pp. 3471–3495, 1974.

[21] (STAR), J. Adam, *et al.*, "Nonmonotonic Energy Dependence of Net-Proton Number Fluctuations," *Phys. Rev. Lett.*, vol. 126, no. 9, p. 092301, 2021.

[22] (STAR), M. Abdallah, *et al.*, "Cumulants and correlation functions of net-proton, proton, and antiproton multiplicity distributions in Au+Au collisions at energies available at the BNL Relativistic Heavy Ion Collider," *Phys. Rev. C*, vol. 104, no. 2, p. 024902, 2021.

[23] (STAR), B. Aboona, *et al.*, "Beam Energy Dependence of Fifth and Sixth-Order Net-proton Number Fluctuations in Au+Au Collisions at RHIC," *Phys. Rev. Lett.*, vol. 130, no. 8, p. 082301, 2023.

[24] (NA61/SHINE), H. Adhikary, *et al.*, "Search for the critical point of strongly-interacting matter in ^{40}Ar + ^{45}Sc collisions at 150A GeV/c using scaled factorial moments of protons," 5 2023. arXiv:2305.07557.

[25] (NA61/SHINE), A. Acharya, *et al.*, "Measurements of π^- production in ^{7}Be+^{9}Be collisions at beam momenta from 19A to 150AGeV/c in the NA61/SHINE experiment at the CERN SPS," *Eur. Phys. J. C*, vol. 80, no. 10, p. 961, 2020. [Erratum: Eur.Phys.J.C 81, 144 (2021)].

[26] M. Gazdzicki, "Phase diagram of strongly interacting matter: the last 20 years at the CERN SPS," *Eur. Phys. J. ST*, vol. 229, no. 22-23, pp. 3507–3516, 2020.

[27] (CBM), T. Ablyazimov, *et al.*, "Challenges in QCD matter physics –The scientific programme of the Compressed Baryonic Matter experiment at FAIR," *Eur. Phys. J. A*, vol. 53, no. 3, p. 60, 2017.

[28] A. Bzdak, V. Koch, D. Oliinychenko, and J. Steinheimer, "Large proton cumulants from the superposition of ordinary multiplicity distributions," *Phys. Rev. C*, vol. 98, no. 5, p. 054901, 2018.

[29] S. Jeon and V. Koch, "Charged particle ratio fluctuation as a signal for QGP," *Phys. Rev. Lett.*, vol. 85, pp. 2076–2079, 2000.

[30] X. Luo and N. Xu, "Search for the QCD Critical Point with Fluctuations of Conserved Quantities in Relativistic Heavy-Ion Collisions at RHIC : An Overview," *Nucl. Sci. Tech.*, vol. 28, no. 8, p. 112, 2017.

[31] X.-F. Luo, B. Mohanty, H. G. Ritter, and N. Xu, "Search for the QCD Critical Point: Higher Moments of Net-proton Multiplicity Distributions," *Phys. Atom. Nucl.*, vol. 75, p. 676, 2012.

[32] M. Asakawa, U. W. Heinz, and B. Muller, "Fluctuation probes of quark deconfinement," *Phys. Rev. Lett.*, vol. 85, pp. 2072–2075, 2000.

[33] M. I. Gorenstein, M. Gazdzicki, and O. S. Zozulya, "Fluctuations of strangeness and deconfinement phase transition in nucleus nucleus collisions," *Phys. Lett. B*, vol. 585, pp. 237–242, 2004.

[34] V. Koch, A. Majumder, and J. Randrup, "Baryon-strangeness correlations: A Diagnostic of strongly interacting matter," *Phys. Rev. Lett.*, vol. 95, p. 182301, 2005.

[35] M. A. Stephanov, "Non-Gaussian fluctuations near the QCD critical point," *Phys. Rev. Lett.*, vol. 102, p. 032301, 2009.

[36] M. Cheng *et al.*, "Baryon Number, Strangeness and Electric Charge Fluctuations in QCD at High Temperature," *Phys. Rev. D*, vol. 79, p. 074505, 2009.

[37] W.-j. Fu, Y.-x. Liu, and Y.-L. Wu, "Fluctuations and Correlations of Conserved Charges in QCD at Finite Temperature with Effective Models," *Phys. Rev. D*, vol. 81, p. 014028, 2010.

[38] M. A. Stephanov, "On the sign of kurtosis near the QCD critical point," *Phys. Rev. Lett.*, vol. 107, p. 052301, 2011.

[39] V. Skokov, B. Friman, and K. Redlich, "Quark number fluctuations in the Polyakov loop-extended quark-meson model at finite baryon density," *Phys. Rev. C*, vol. 83, p. 054904, 2011.

[40] C. Herold, M. Nahrgang, Y. Yan, and C. Kobdaj, "Dynamical net-proton fluctuations near a QCD critical point," *Phys. Rev. C*, vol. 93, no. 2, p. 021902, 2016.

[41] M. Szymański, M. Bluhm, K. Redlich, and C. Sasaki, "Net-proton number fluctuations in the presence of the QCD critical point," *J. Phys. G*, vol. 47, no. 4, p. 045102, 2020.

[42] W. Broniowski and A. Olszewski, "Statistical moments in superposition models and strongly intensive measures," *Phys. Rev. C*, vol. 95, no. 6, p. 064910, 2017.

[43] A. Bialas and V. Koch, "Event by event fluctuations and inclusive distribution," *Phys. Lett. B*, vol. 456, pp. 1–4, 1999.

[44] B. Friman, F. Karsch, K. Redlich, and V. Skokov, "Fluctuations as probe of the QCD phase transition and freeze-out in heavy ion collisions at LHC and RHIC," *Eur. Phys. J. C*, vol. 71, p. 1694, 2011.

[45] V. Vovchenko, R. V. Poberezhnyuk, D. V. Anchishkin, and M. I. Gorenstein, "Non-Gaussian particle number fluctuations in vicinity of the critical point for van der Waals equation of state," *J. Phys. A*, vol. 49, no. 1, p. 015003, 2016.

[46] S. Borsanyi, Z. Fodor, J. N. Guenther, S. K. Katz, K. K. Szabo, A. Pasztor, I. Portillo, and C. Ratti, "Higher order fluctuations and correlations of conserved charges from lattice QCD," *JHEP*, vol. 10, p. 205, 2018.

[47] (STAR), L. Adamczyk, *et al.*, "Collision Energy Dependence of Moments of Net-Kaon Multiplicity Distributions at RHIC," *Phys. Lett. B*, vol. 785, pp. 551–560, 2018.

[48] N. K. Behera (ALICE), "Higher moment fluctuations of identified particle distributions from ALICE," *Nucl. Phys. A*, vol. 982, pp. 851–854, 2019.

[49] (PHENIX), A. Adare, *et al.*, "Measurement of higher cumulants of net-charge multiplicity distributions in Au+Au collisions at $\sqrt{s_{NN}} = 7.7 - 200$ GeV," *Phys. Rev. C*, vol. 93, no. 1, p. 011901, 2016.

[50] (STAR), L. Adamczyk, *et al.*, "Energy Dependence of Moments of Net-proton Multiplicity Distributions at RHIC," *Phys. Rev. Lett.*, vol. 112, p. 032302, 2014.

[51] X. Luo (STAR), "Energy Dependence of Moments of Net-Proton and Net-Charge Multiplicity Distributions at STAR," *PoS*, vol. CPOD2014, p. 019, 2015.

[52] (STAR), M. S. Abdallah, *et al.*, "Measurements of Proton High Order Cumulants in $\sqrt{s_{\rm NN}}$ = 3 GeV Au+Au Collisions and Implications for the QCD Critical Point," *Phys. Rev. Lett.*, vol. 128, no. 20, p. 202303, 2022.

[53] B. Ling and M. A. Stephanov, "Acceptance dependence of fluctuation measures near the QCD critical point," *Phys. Rev. C*, vol. 93, no. 3, p. 034915, 2016.

[54] A. Bzdak, V. Koch, and N. Strodthoff, "Cumulants and correlation functions versus the QCD phase diagram," *Phys. Rev. C*, vol. 95, no. 5, p. 054906, 2017.

[55] A. Bzdak and V. Koch, "Mapping the QCD phase diagram with statistics friendly distributions," *Phys. Rev. C*, vol. 100, no. 5, p. 051902, 2019.

[56] A. Bzdak and P. Bozek, "Multiparticle long-range rapidity correlations from fluctuation of the fireball longitudinal shape," *Phys. Rev. C*, vol. 93, no. 2, p. 024903, 2016.

[57] B. Friman and K. Redlich, "Fluctuations in the canonical ensemble of an Abelian charge," 5 2022. arXiv: 2205.07332.

[58] (HADES), J. Adamczewski-Musch, *et al.*, "Proton-number fluctuations in $\sqrt{s_{NN}}$ =2.4 GeV Au + Au collisions studied with the High-Acceptance DiElectron Spectrometer (HADES)," *Phys. Rev. C*, vol. 102, no. 2, p. 024914, 2020.

[59] (STAR), M. Abdallah, *et al.*, "Higher-order cumulants and correlation functions of proton multiplicity distributions in sNN=3 GeV Au+Au collisions at the RHIC STAR experiment," *Phys. Rev. C*, vol. 107, no. 2, p. 024908, 2023.

[60] M. A. Stephanov, K. Rajagopal, and E. V. Shuryak, "Event-by-event fluctuations in heavy ion collisions and the QCD critical point," *Phys. Rev. D*, vol. 60, p. 114028, 1999.

[61] C. Athanasiou, K. Rajagopal, and M. Stephanov, "Using Higher Moments of Fluctuations and their Ratios in the Search for the QCD Critical Point," *Phys. Rev. D*, vol. 82, p. 074008, 2010.

[62] A. Marcinek (NA61/SHINE), "Highlights from the NA61/SHINE Experiment," *Acta Phys. Polon. Supp.*, vol. 16, no. 1, p. 8, 2023.

[63] A. Seryakov (NA61/SHINE), "Rapid change of multiplicity fluctuations in system size dependence at SPS energies," *KnE Energ. Phys.*, vol. 3, pp. 170–177, 2018.

[64] M. Barej and A. Bzdak, "Cumulants from fluctuating width of rapidity distribution," *Phys. Rev. C*, vol. 108, no. 1, p. 014907, 2023.

[65] V. Skokov, B. Friman, and K. Redlich, "Volume Fluctuations and Higher Order Cumulants of the Net Baryon Number," *Phys. Rev. C*, vol. 88, p. 034911, 2013.

[66] R. J. Glauber, "Cross-sections in deuterium at high-energies," *Phys. Rev.*, vol. 100, pp. 242–248, 1955.

[67] A. Bialas, M. Bleszynski, and W. Czyz, "Multiplicity Distributions in Nucleus-Nucleus Collisions at High-Energies," *Nucl. Phys. B*, vol. 111, pp. 461–476, 1976.

[68] M. L. Miller, K. Reygers, S. J. Sanders, and P. Steinberg, "Glauber modeling in high energy nuclear collisions," *Ann. Rev. Nucl. Part. Sci.*, vol. 57, pp. 205–243, 2007.

[69] C. Loizides, J. Nagle, and P. Steinberg, "Improved version of the PHOBOS Glauber Monte Carlo," *SoftwareX*, vol. 1-2, pp. 13–18, 2015.

[70] A. Bzdak, V. Koch, and V. Skokov, "Correlated stopping, proton clusters and higher order proton cumulants," *Eur. Phys. J. C*, vol. 77, no. 5, p. 288, 2017.

[71] M. Barej, A. Bzdak, and P. Gutowski, "Wounded nucleon, quark, and quark-diquark emission functions versus experimental results from the BNL Relativistic Heavy Ion Collider at $\sqrt{s_{NN}}$ =200 GeV," *Phys. Rev. C*, vol. 100, no. 6, p. 064902, 2019.

[72] X. Luo, J. Xu, B. Mohanty, and N. Xu, "Volume fluctuation and auto-correlation effects in the moment analysis of net-proton multiplicity distributions in heavy-ion collisions," *J. Phys. G*, vol. 40, p. 105104, 2013.

[73] M. Gazdzicki and S. Mrowczynski, "A Method to study 'equilibration' in nucleus-nucleus collisions," *Z. Phys. C*, vol. 54, pp. 127–132, 1992.

[74] M. I. Gorenstein and M. Gazdzicki, "Strongly Intensive Quantities," *Phys. Rev. C*, vol. 84, p. 014904, 2011.

[75] I. A. Sputowska, "Forward-backward correlations with the Σ quantity in the wounded-constituent framework at energies available at the CERN Large Hadron Collider," *Phys. Rev. C*, vol. 108, no. 1, p. 014903, 2023.

[76] A. Bzdak, V. Koch, and V. Skokov, "Baryon number conservation and the cumulants of the net proton distribution," *Phys. Rev. C*, vol. 87, no. 1, p. 014901, 2013.

[77] P. Braun-Munzinger, B. Friman, K. Redlich, A. Rustamov, and J. Stachel, "Relativistic nuclear collisions: Establishing a non-critical baseline for fluctuation measurements," *Nucl. Phys. A*, vol. 1008, p. 122141, 2021.

[78] V. Vovchenko, O. Savchuk, R. V. Poberezhnyuk, M. I. Gorenstein, and V. Koch, "Connecting fluctuation measurements in heavy-ion collisions with the grand-canonical susceptibilities," *Phys. Lett. B*, vol. 811, p. 135868, 2020.

[79] V. Vovchenko, V. Koch, and C. Shen, "Proton number cumulants and correlation functions in Au-Au collisions at sNN=7.7–200 GeV from hydrodynamics," *Phys. Rev. C*, vol. 105, no. 1, p. 014904, 2022.

[80] (ALICE), S. Acharya, *et al.*, "Global baryon number conservation encoded in net-proton fluctuations measured in Pb-Pb collisions at $\sqrt{s_{\rm NN}}$ = 2.76 TeV," *Phys. Lett. B*, vol. 807, p. 135564, 2020.

[81] O. Savchuk, V. Vovchenko, V. Koch, J. Steinheimer, and H. Stoecker, "Constraining baryon annihilation in the hadronic phase of heavy-ion collisions via event-by-event fluctuations," *Phys. Lett. B*, vol. 827, p. 136983, 2022.

[82] R. V. Poberezhnyuk, O. Savchuk, M. I. Gorenstein, V. Vovchenko, K. Taradiy, V. V. Begun, L. Satarov, J. Steinheimer, and H. Stoecker, "Critical point fluctuations: Finite size and global charge conservation effects," *Phys. Rev. C*, vol. 102, no. 2, p. 024908, 2020.

[83] V. A. Kuznietsov, O. Savchuk, M. I. Gorenstein, V. Koch, and V. Vovchenko, "Critical point particle number fluctuations from molecular dynamics," *Phys. Rev. C*, vol. 105, no. 4, p. 044903, 2022.

[84] Wolfram Research Inc., "Mathematica, version 12.0.0.0." `https://www.wolfram.com/mathematica/`. accessed: 25.05.2023.

[85] J. D. Hunter, "Matplotlib: A 2d graphics environment," *Computing in Science & Engineering*, vol. 9, no. 3, pp. 90–95, 2007.

[86] M. Barej and A. Bzdak, "Factorial cumulants from global baryon number conservation," *Phys. Rev. C*, vol. 102, no. 6, p. 064908, 2020.

[87] M. Barej and A. Bzdak, "Factorial cumulants from short-range correlations and global baryon number conservation," *Phys. Rev. C*, vol. 106, no. 2, p. 024904, 2022.

[88] M. Barej and A. Bzdak, "Cumulants from short-range correlations and baryon number conservation at next-to-leading order," *Phys. Rev. C*, vol. 107, no. 3, p. 034914, 2023.

[89] K. Pearson, "Ix. mathematical contributions to the theory of evolution.—xix. second supplement to a memoir on skew variation," *Philosophical Transactions of the Royal Society of London. Series A, Containing Papers of a Mathematical or Physical Character*, vol. 216, no. 538-548, pp. 429–457, 1916.

[90] A. Bzdak and D. Teaney, "Longitudinal fluctuations of the fireball density in heavy-ion collisions," *Phys. Rev. C*, vol. 87, no. 2, p. 024906, 2013.

[91] J. Jia, S. Radhakrishnan, and M. Zhou, "Forward-backward multiplicity fluctuation and longitudinal harmonics in high-energy nuclear collisions," *Phys. Rev. C*, vol. 93, no. 4, p. 044905, 2016.

[92] M. Rohrmoser and W. Broniowski, "Longitudinal correlations from fluctuating strings in Pb-Pb, p-Pb, and p-p collisions," *Phys. Rev. C*, vol. 101, no. 1, p. 014907, 2020.

[93] (ATLAS), M. Aaboud, *et al.*, "Measurement of forward-backward multiplicity correlations in lead-lead, proton-lead, and proton-proton collisions with the ATLAS detector," *Phys. Rev. C*, vol. 95, no. 6, p. 064914, 2017.

[94] (ALICE), S. Acharya, *et al.*, "Longitudinal asymmetry and its effect on pseudorapidity distributions in Pb-Pb collisions at $\sqrt{s_{NN}}$ = 2.76 TeV," *Phys. Lett. B*, vol. 781, pp. 20–32, 2018.

[95] R. Quishpe, "Longitudinal Fluctuations in Relativistic Heavy Ion Collisions," 2022. `https://cds.cern.ch/record/2835858/files/CERN-THESIS-2022-145.pdf`, Doctoral thesis presented 18 Jan 2022; Accessed: 02-05-2023.

[96] B. Kimelman (STAR), "Baryon Stopping and Associated Production of Mesons in Au+Au Collisions at $\sqrt{s_{NN}} = 3.0$ GeV at STAR," *Acta Phys. Polon. Supp.*, vol. 16, no. 1, p. 49, 2023.

Appendix A

Supplemental information

A.1 Conference activity

1. **M. Barej***, A. Bzdak, *Cumulants with global baryon conservation and short-range correlations*, 22nd Zimanyi School Winter Workshop on Heavy Ion Physics, 05-09 December 2022, Budapest, Hungary **(poster)**

2. **M. Barej***, A. Bzdak, *Cumulants from global baryon number conservation with short-range correlations*, CPOD2022 - Workshop on Critical Point and Onset of Deconfinement, 28 November - 02 December 2022, online **(oral)**

3. **M. Barej***, A. Bzdak, *Correlations from short-range correlations and global baryon number conservation*, 11th International Conference on New Frontiers in Physics, 30 August - 12 September 2022, Kolymbari, Greece / online **(oral)**

4. **M. Barej***, A. Bzdak, *QCD phase diagram and factorial cumulants*, IFJ PAN Particle Physics Summer Student Alumni Conference 2022, 09-10 July 2022, Kraków, Poland **(oral)**

5. **M. Barej***, A. Bzdak, *Correlations from global baryon number conservation*, 29th International Conference on Ultrarelativistic Nucleus-Nucleus Collisions Quark Matter, 04 - 10 April 2022, Kraków, Poland **(poster)**

6. **M. Barej***, A. Bzdak, *Correlations generated by global baryon number conservation*, 10th International Conference on New Frontiers in Physics, 23 August - 07 September 2021, Kolymbari, Greece / online **(oral)**

7. **M. Barej***, A. Bzdak, P. Gutowski, *Wounded quarks, diquarks, and nucleons in heavy-ion collisions*, 19th Zimanyi School Winter Workshop on Heavy Ion Physics, 02-06 December 2019, Budapest, Hungary **(oral)**

* Speaker or presenting author.

A.2 Publications not included in the thesis

During PhD studies

1. D. Dominik, R. Staszewski, M. Trzebinski, B. Dixit, A. Mavrantoni, M. Juzek, **M. Barej**, P. Erland, I. Babiarz and J. J. Malczewski, *et al.*, *Proceedings of the IFJ PAN Particle Physics Summer Student Alumni Conference 2022*. DOI:10.48733/978-83-63542-30-6

2. **M. Barej**, A. Bzdak and P. Gutowski, *Wounded nucleon, quark, and quark-diquark emission functions versus experimental results from the BNL Relativistic Heavy Ion Collider at* $\sqrt{s_{NN}}$ *=200 GeV*, Phys. Rev. C 100, no.6, 064902 (2019). DOI:10.1103/PhysRevC.100.064902

Before PhD studies

1. P. Gutowski, **M. Barej** and A. Bzdak, *Wounded Source Models Versus Experimental Results from RHIC*, Acta Phys. Polon. B 50, 1071-1076 (2019). DOI:10.5506/APhysPolB.50.1071

2. **M. Barej**, A. Bzdak and P. Gutowski, *Wounded-quark emission function at the top energy available at the BNL Relativistic Heavy Ion Collider*, Phys. Rev. C 97, no.3, 034901 (2018). DOI:10.1103/PhysRevC.97.034901

A.3 Internships

1. **Summer school**, National Nuclear Physics Summer School, Massachusetts Institute of Technology (MIT), Cambridge, Massachusetts, United States, 11-22 July 2022.

2. **Winter school**, Frontiers in Nuclear and Hadronic Physics, The Galileo Galilei Institute For Theoretical Physics, Florence, Italy, 24-28 February 2020.

A.4 Grants and projects

1. Co-investigator in the National Science Center (NCN, Poland) SHENG 1 grant: *Dynamics of hot QCD matter in heavy ion collisions: from small to large systems*, 2018/30/Q/ST2/00101, 2019-2023.

A.5 Awards

1. The Arkadiusz Piekara Master's Award of the Polish Physical Society (Polskie Towarzystwo Fizyczne, PTF) for the best master thesis (2020).

2. Quality-related scholarships for the best doctoral students, Excellence Initiative - Research University (IDUB), AGH University of Kraków (twice: 2021/2022, 2022/2023).

3. Scholarship for doctoral students for scientific achievements, AGH University of Kraków (twice: 2021/2022, 2022/2023).

A.6 Other scientific activities

1. Oral talk, *Search for the QCD Phase Transition with Factorial Cumulants*, Heavy Ion Physics Seminar "Białasówka", Kraków, Poland (2023).

2. Oral talk, *Wounded quarks in heavy-ion collisions*, Heavy Ion Physics Seminar "Białasówka", Kraków, Poland (2019).

3. Teaching students: Physics II - laboratory classes (2 groups in 2020/2021 and 3 groups in 2022/2023) at AGH University of Kraków.

Appendix B

Published articles